Available online at www.sciencedirect.com
SCIENCE DIRECT
Thermochimica Acta 442 (2006) 35–41
thermochimica acta
www.elsevier.com/locate/tca

The heat capacity of polyethylene fibers measured by multi-frequency temperature-modulated calorimetry

M. Pyda [a,b,c,*], E. Nowak-Pyda [a], B. Wunderlich [a,b]

[a] *Department of Chemistry, The University of Tennessee, Knoxville, TN 37996-1600, USA*
[b] *Chemical Sciences Division, Oak Ridge National Laboratory, Oak Ridge, TN 37831-6197, USA*
[c] *Department of Chemistry, The University of Technology Rzeszow, 35959 Rzeszow, Poland*

Available online 4 January 2006

Abstract

The apparent heat capacity of polyethylene fibers in the melting region was measured by quasi-isothermal, temperature-modulated differential scanning calorimetry (TMDSC) and compared with results from standard differential scanning calorimetry (DSC) and the solid and liquid thermodynamic heat capacity as references from the ATHAS Data Bank. Using a multi-frequency, complex sawtooth modulation in the quasi-isothermal mode disclosed for the first time that the uncorrected apparent heat capacity $C_p = A_\Phi/(A_{T_s}\omega)$ of the liquid polyethylene fiber increases with increasing frequency (A_Φ is the differential heat-flow rate and A_{T_s} is the sample temperature). The frequency-dependent heat capacity cannot be represented by the expression: $C_p = A_\Phi/(A_{T_s}\nu\omega)[1 + (\tau\nu\omega)^2]^{0.5}$ because of a negative τ^2. The results were later confirmed by independent measurements on single sinusoidal quasi-isothermal TMDSC on the same material. The error is caused by shrinking of the fiber, which deforms the sample pan.

Keywords: Heat capacity; Polyethylene fiber; Temperature-modulated differential scanning calorimetry; Higher harmonics; Multi-frequency sawtooth modulation

1. Introduction

Experimental heat capacities of gel-spun fibers of ultrahigh-molar-mass polyethylene (PE) are presented in the literature with unexpected high values in the premelting region [1,2]. Repeating these measurements shows that an error of estimating C_p was made by applying the same calibration for the solid and liquid states of the fiber. In the liquid state, the experimental C_p was observed to be lower than the expected value from the ATHAS Data Bank [3]. This lower C_p resulted from the shrinkage of the fibers which causes a lateral expansion and deformed the bottom of the pan. In this paper, the difficulties in the estimation of heat capacity of PE fiber in the liquid state with multi-frequency, temperature-modulated DSC are presented and compared with results from standard DSC and quasi-isothermal TMDSC with single sinusoidal temperature modulation.

Three techniques: adiabatic calorimetry, standard differential scanning calorimetry (DSC), and temperature-modulated differential scanning calorimetry (TMDSC) can be used to determine the apparent heat capacity, $C_p^* = C_p + (\partial L/\partial n)_{p,T}$. The thermodynamic heat capacity, $C_p = (\partial H/\partial T)_{n,p}$ represents the change in heat content, H, with temperature, T, at constant composition, n, and pressure, p, while L is the latent heat, connected to additional processes like heat of melting, cold crystallization, or reorganization.

With standard DSC, assumed to be at steady state, the difference in temperature between reference and sample ($T_r - T_s = \Delta T$) is directly proportional to the heat-flow rate, $\Phi = \Delta T \times K$ so that $C_p = \Phi/q$, where K is determined by calibration with a standard, such as sapphire (Al_2O_3) and q is heating rate. A typical precision of up to 3% is possible in such measurements.

In TMDSC, the programmed temperature is produced by superposition of a temperature modulation on the constant heating rate [4]. The common modulations applied for TMDSC are sinusoidal, sawtooth-like, or step-isothermal. Measurements, however, can also be made in the quasi-isothermal mode, i.e., with an underlying heating rate $\langle q \rangle = 0$ [5,6]. In the quasi-isothermal method of TMDSC, a reversing heat capacity can be evaluated from the amplitudes of the heat-flow rate A_Φ, the corresponding sample temperature, A_{T_s}, and the frequency, ω [7]:

$$C_p = \frac{A_\Phi}{A_{T_s}\omega} K(\omega), \tag{1}$$

* Corresponding author.
E-mail address: mpyda@utk.edu (M. Pyda).

0040-6031/$ – see front matter © 2005 Elsevier B.V. All rights reserved.
doi:10.1016/j.tca.2005.11.014

where ω is the frequency in rad s^{-1} ($\omega = 2\pi/p$, with p representing in this case the modulation period in s) and $K(\omega) = [1 + (C_r\omega/K)^2]^{0.5}$ corrects for the different modulation frequencies, with C_r representing the heat capacity of the reference calorimeter and K, Newton's law constant as in the DSC equation, given in the above text. Note that $A_{T_s}\omega$ is the amplitude of the heating rate, dT/dt. Amplitudes are extracted from the raw data, gathered as a function of time, in terms of the first harmonic by Fourier transforms from the time to the frequency domain. For calorimetry outside of the transition regions, the total and the reversing heat capacities are identical. Within transition regions a non-reversing heat capacity is observed as the difference between total and reversing heat capacities. In case the reversing signal is constant over long times, it may be considered reversible.

2. Multi-frequency complex sawtooth modulation

In an extensive study of calorimetry with sawtooth modulation, it was found empirically that Eq. (1) with an adjustable τ could be used for analysis over a wide frequency range, using the data of the first harmonic ($\nu = 1$) and also of higher harmonics ($\nu = 3, 5, 7, \ldots$) [5,6]:

$$C_p = \frac{A_{HF}(\nu)}{A_{T_s}(\nu)\nu\omega} K(\nu\omega), \tag{2}$$

where the correction function $K(\nu\omega)$ in Eq. (2) is of the form:

$$K(\nu\omega) = \sqrt{1 + \tau^2(\nu\omega)^2}, \tag{3}$$

and where τ is an empirical function, which becomes constant and under the conditions of steady state, linearity, and stationarity of response.

A simple, centrosymmetric sawtooth modulation about T_0 can be described by the Fourier series:

$$T(t) - T_0 = \frac{8A}{\pi^2}\left[\sin\omega t - \frac{1}{9}\sin 3\omega t + \frac{1}{25}\sin 5\omega t - \frac{1}{49}\sin 7\omega t + \frac{1}{81}\sin 9\omega t - \cdots\right], \tag{4}$$

where A is the modulation amplitude. Only the first harmonic in Eq. (4) has a big amplitude, the other amplitudes decrease quickly with frequency. Calculations of the heat capacities from the higher harmonics have, thus, less precision, still they can be used for heat capacity evaluation [5,6].

In order to improve the evaluation heat capacity from higher harmonic components, a complex sawtooth with identical harmonics for $\nu = 1$, 3, 5, and 7 was generated [7]:

$$T_y(t) - T_0 = \frac{8A}{\pi^2}\left[\sin\omega t + \sin 3\omega t + \sin 5\omega t + \sin 7\omega t - \frac{1}{9}\sin 9\omega t - \cdots\right]. \tag{5}$$

This complex sawtooth can be approximated by 26 straight segments. Next, a simplified complex sawtooth of 14 segments $T_x(t)$ was proposed with close to equal amplitudes for the four harmonics of the Fourier series of Eq. (5). An example run with sapphire is shown in Fig. 1 and its Fourier series is given by [7]:

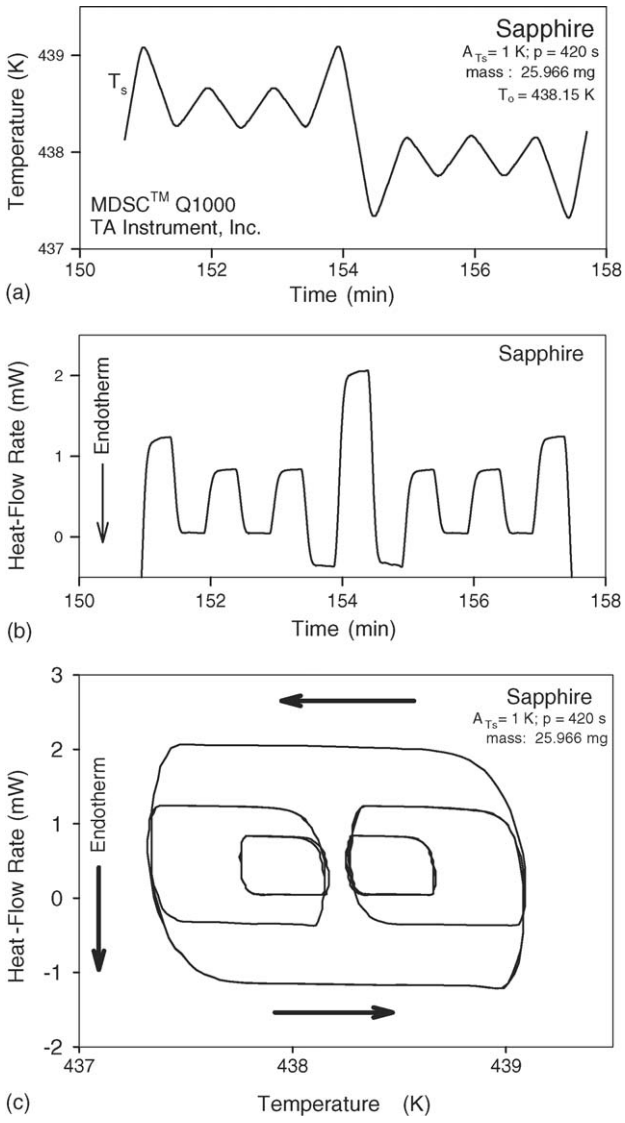

Fig. 1. Example of a calibration run using the simplified, complex sawtooth of Eq. (6). The curves show (a) the sample temperature $T_s(t)$, (b) the heat-flow rate, and (c) the Lissajous figure, i.e., the change of the heat-flow rate plotted against the change of the sample temperature.

$$T_x(t) - T_0 = \frac{8A}{\pi^2}[0.378\sin\omega t + 0.251\sin 3\omega t + 0.217\sin 5\omega t + 0.348\sin 7\omega t + \cdots]. \tag{6}$$

This simplified complex sawtooth with an overall period of 420 s (30 s per sub-segment) was applied for the analysis of the PE fiber and the results were computed using Eqs. (2) and (3).

It was shown in Ref. [8] that it is possible to produce this complex sawtooth with a standard DSC and to determine the various sinusoidal Fourier components to obtain simultaneous information on the sample response to modulation with different frequencies. It is shown in this paper that in the new Q1000® DSC of TA Instrument makes a considerable progress

in reaching steady state. Similar data were previously derived for a power-compensated TMDSC [5,6,9]. Results are given for sapphire and polyethylene fibers.

3. Experimental

3.1. Samples

The sample measured in this paper, and called PE fiber, is a gel-spun fiber of ultrahigh-molar-mass polyethylene (UHMM-PE) with molar mass of $M_w > 10^6$ Da, supplied by Allied-Signal Inc. This sample is of the commercial type Spectra 900TM, and is identical to the PE-III fiber, used earlier for a detailed thermodynamic analysis [10]. The samples were placed in aluminum pans of 20 μm thickness provided by TA Instruments Inc. The pan-weights of 23.0 mg for sample and reference pans were matched within ±0.05 mg. The fibers were aligned parallel within the pan using a method developed before [11]. Measurements were carried out with 2.629 mg of the polyethylene fiber. Single-crystalline sapphire was used for the final heat capacity calibrations, its sample mass was 25.966 mg.

3.2. Instrumentation

A DSC of the Q1000® series of TA Instrument Inc. was used for all temperature-modulated and standard DSC measurements. Dry nitrogen gas with a flow rate of 10 mL min^{-1} was purged to the cell. Cooling was supplied to 185 K with a mechanical refrigerator. Dry nitrogen gas with a flow rate of 10 mL min^{-1} was purged through the DSC cell and cooling to 185 K was achieved with a refrigerated cooling system. The sample temperatures were calibrated in the common manner using the onset temperatures of the melting of indium (429.75 K) and water (273.15 K) at a heating rate of 10 K min^{-1}. The heat-flow rate was approximately calibrated with the heat of fusion of indium and then corrected at the temperature of measurement with a heat-capacity determination on sapphire. The heat-flow rate of the empty calorimeter was corrected with the standard Tzero® calibration method of the Q1000® [12] for all data presented. The standard DSC was performed by heating at 10 K min^{-1}. It was used for a first run of the PE fiber to establish the crystallinity.

For the multi-frequency experiments, quasi-isothermal TMDSC with a complex sawtooth modulation was run in the standard DSC mode of operation. The complex sawtooth is described by Eq. (6), and an example is shown in Fig. 1. Each sub-segment had a time of 30 s and the harmonics with $\nu = 1$, 3, 5, 7, and 9 correspond to periods p of 420, 140, 84, 60, and 46.667 s, respectively. The quasi-isothermally experiments with the complex sawtooth modulation were performed at 308.15 and 438.15 K for sapphire and the PE fiber. An asymmetry run of two empty pans was added for the evaluation of the data independent of the TA Instrument software. Each of the experiments consisted of 15 cycles. The Lissajous figure of Fig. 1c, for example, is a superposition of the last 10 cycles of the sapphire run at 438.15 K. For each sub-cycle, the heat-flow rate ultimately reached steady state.

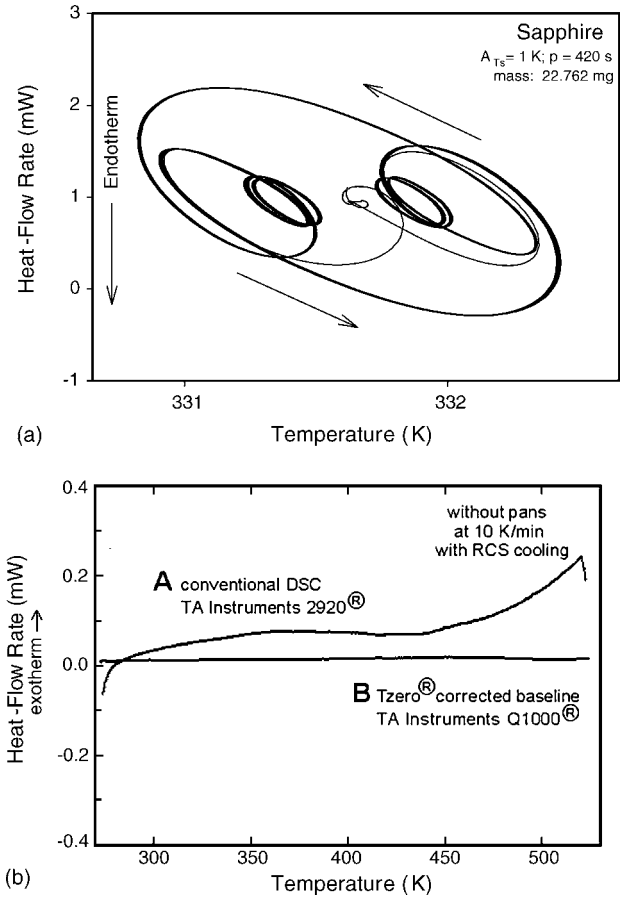

Fig. 2. Lissajous figure from a run with the DSC 2920® under similar conditions as seen in Fig. 1 for the DSC Q1000® (a). The bottom graph (b) shows a comparison of baseline runs obtained without pans using the TA Instrument DSC 2920® (curve A) and the DSC Q1000® after Tzero® calibration (curve B).

In addition, quasi-isothermal TMDSC was done also at a series of temperatures with simple sinusoidal modulation, using an amplitude of 0.5 K and a period of 60 s. These runs lasted for 30 min at each chosen temperature, and data were collected from the last 10 min.

Fig. 2 illustrates the improvement of the Tzero®-calibrated Q1000® over the DSC 2920® used earlier [8]. Fig. 2a allows a comparison with the Lissajous figure of the DSC 2920® with the performance of the Q1000®, shown in Fig. 1c. The rounding of the corners in Fig. 1c and the corresponding shapes in Fig. 2a are measures of the times it takes to reach steady state in each segment of the complex sawtooth. On instantaneous response, the Lissajous shapes should have square corners. Despite the slower attainment of steady state of the DSC 2920® in Fig. 2a, linearity between temperature and heat-flow rate was preserved and heat capacities could be measured to a precision exceeding standard DSC [8]. Fig. 2b illustrates deviations in heat-flow rate of less than 0.05 mW between 185 and 670 K for the Q1000®. In addition, the asymmetry of the baseline is small enough, to make additional asymmetry corrections unnecessary. This is a major advantage over the DSC 2920® and most other heat-flux and power-compensation DSCs since the asymmetry correction involves a phase shift which allows only approximate correction [13,14].

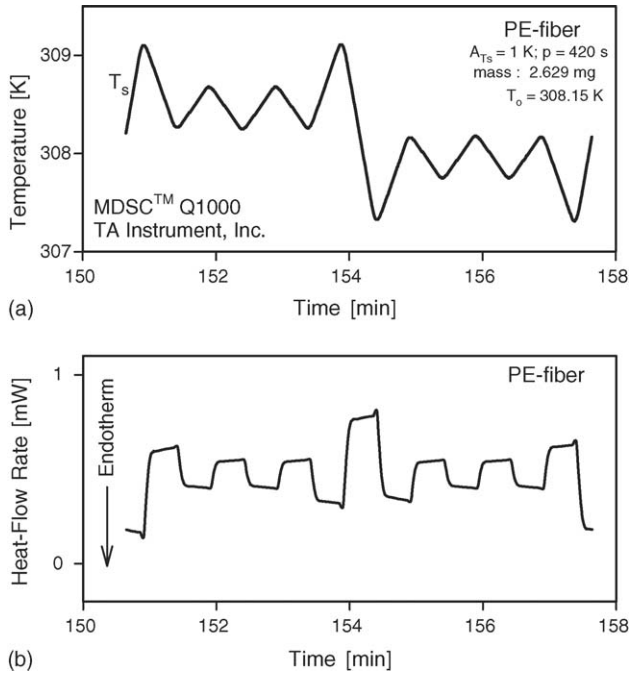

Fig. 3. Polyethylene measured in the premelting region. (a) Data for the sample temperature $T_s(t)$. (b) Data of the heat-flow rate. Complex sawtooth modulation.

3.3. Calculations

Only the raw data as generated by the standard DSC mode of the Q1000® DSC were collected. All further calculations were performed with our own software, based on Mathematica 3.0™. The calculation of the heat capacity, C_p, from the various harmonics of Eq. (2) requires the evaluation of each harmonic, ν, for the amplitudes of the heat-flow rate, $A_\Phi(\nu)$, and the sample temperature, $A_{T_s}(\nu)$, and evaluation of $K(\nu\omega)$ by using Eq. (3). The time constant τ and corrected heat capacity, C_p(c), can be obtained by setting $K(\nu\omega)$ equal to one, and then plotting the inverse of the squared, uncorrected heat capacity, C_p(uc) versus the square of the frequency, $(\nu\omega)^2$. The slope of a linear fit yields τ^2 as seen from:

$$\frac{1}{C_p^2(\mathrm{uc})} = \frac{1}{C_p^2(\mathrm{c})} + \frac{\tau^2}{C_p^2(\mathrm{c})}(\nu\omega)^2. \tag{7}$$

The intercept of the plot at $(\nu\omega)^2 = 0$ is directly the inverse of the squared, τ-corrected heat capacity. The final step is the evaluation of the correction factor from the preliminary setting of the heat flow with the indium heat of fusion by comparison with a sapphire experiment. As a result of the export of the raw data from the Q1000® DSC, the Tzero® was not be included in the evaluation, and an asymmetry run had to be used, as before [13].

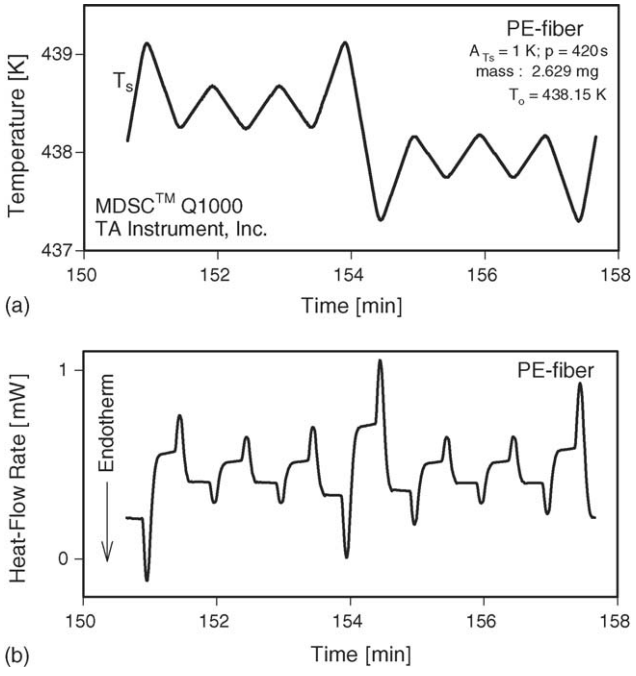

Fig. 4. Polyethylene measured in the liquid region. (a) Data for the sample temperature $T_s(t)$. (b) Data of the heat-flow rate. Complex sawtooth modulation.

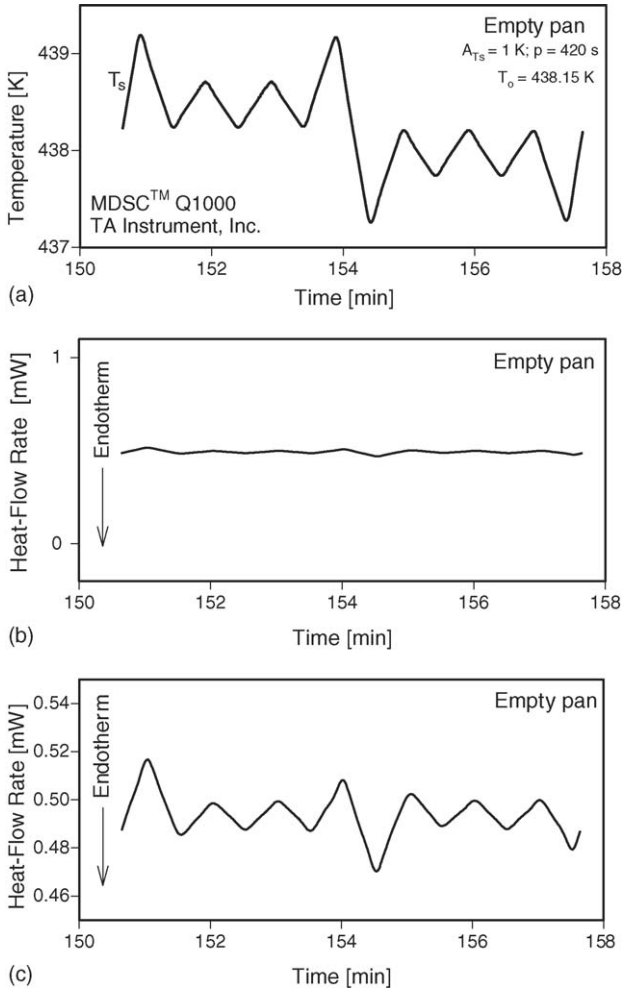

Fig. 5. Measurement on an empty pan at 438.15 K. (a) Data for the sample temperature $T_s(t)$ and the data of the heat-flow rate (b) by complex sawtooth modulation in the liquid region of PE fibers; (c) magnification of the results in (b).

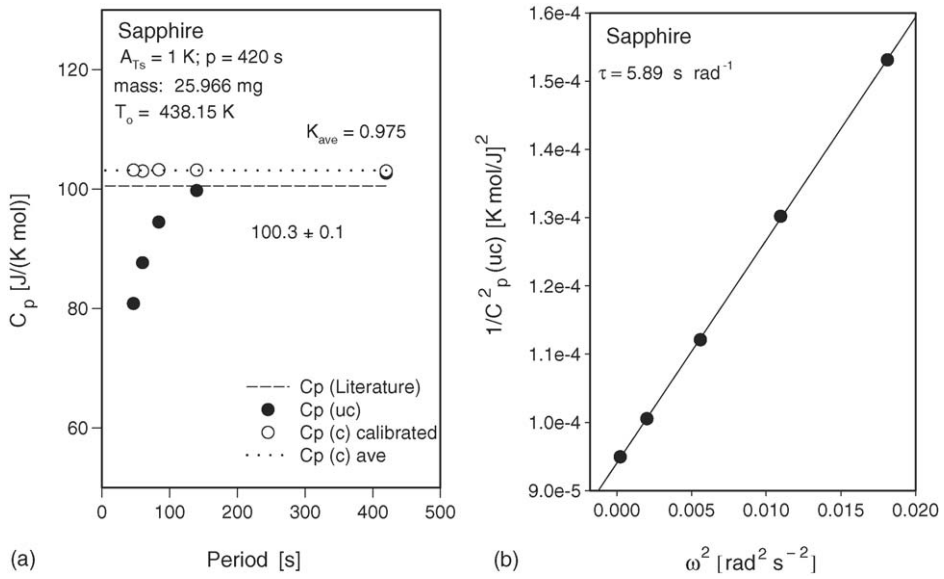

Fig. 6. Analysis of data as shown in Fig. 1 for sapphire at 438.15 K. (a) Plot of the uncorrected and τ-corrected heat capacities. (b) Plot of the uncorrected heat capacities to obtain τ from Eq. (7).

4. Results and discussion

The evaluation of heat capacity of PE fiber in the premelting and liquid regions with TMDSC was carried out with a complex sawtooth modulation to make certain that for all frequencies an identical sample and pan configuration is analyzed. Fig. 3 shows the raw data of sample temperature and heat-flow rate for the PE fiber in the semicrystalline state before major melting, and Fig. 4 in the liquid state. Due to the change in heat-flow-rate response when changing the temperature program from one segment of the complex sawtooth to the other, the observed heat-flow rate at 438.15 K in Fig. 4b contains spikes at the end of every segment of the sawtooth, i.e., in this short time interval the DSC response in non-linear. The spikes must be caused by a substantial lag of the actual temperature within the sample pan behind the programmed temperature measured at the sample thermocouple. This gives an erroneous, lower heat capacity at the beginning of a cooling segment and a higher one at the beginning of the heating segment. The cause of this larger temperature gradient within the sample pan is linked to a major distortion of the sample pan on shrinking of the fiber on melting which expands the fiber diameter substantially [15]. Note that Fig. 3 shows a much smaller effect. In this run, the fiber is not yet melted, and the pan has still in its original flat bottom. The spikes in the heat-flow rate disturb the higher harmonics more than the lower ones.

In Fig. 1 the raw data at 438.15 K of the temperature and the heat-flow rate for sapphire, Al_2O_3, are presented, respectively.

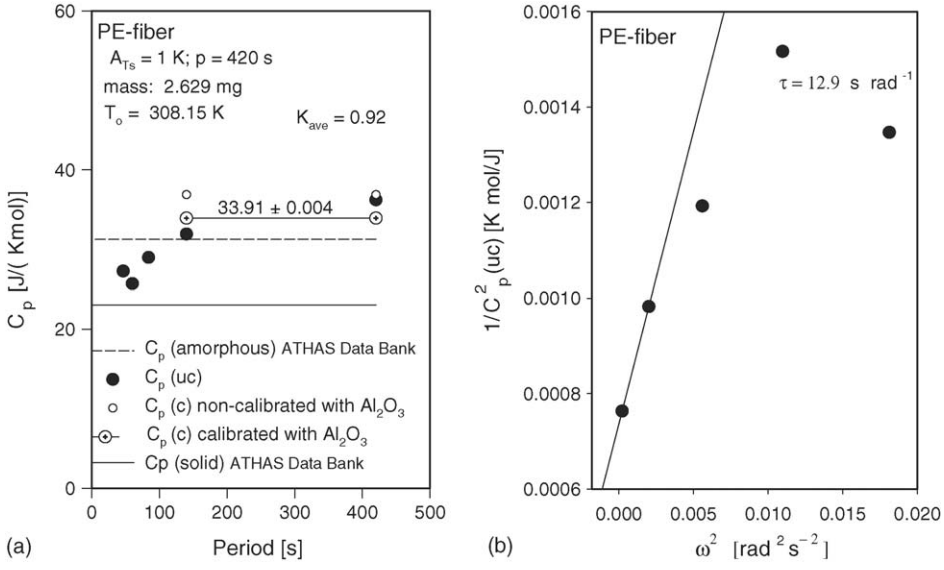

Fig. 7. Analysis of data as shown in Fig. 3 for PE fibers at 308.15 K, before the first melting. (a) Plot of the uncorrected, τ-corrected, and Al_2O_3 calibrated heat capacities. (b) Plot of the uncorrected heat capacities to obtain τ from Eq. (7).

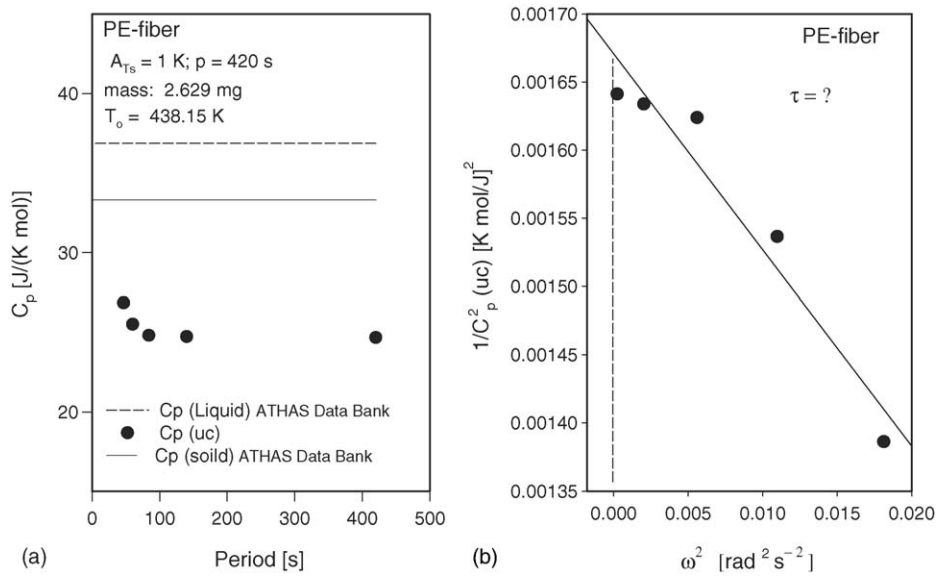

Fig. 8. Analysis of data as shown in Fig. 4 for PE fibers at 438.15 K in the melting region. (a) Plot of the uncorrected heat capacities. (b) Plot of the uncorrected heat capacities in an attempt to obtain τ from Eq. (7).

They are used to establish a calibration of C_p. In addition, Fig. 5 illustrates a run with an empty aluminum pan for the asymmetry correction. No spikes are seen in either set of data. Similar results were obtained for Al_2O_3 and the empty pans at 308.15 K.

In Fig. 6 the Al_2O_3 data at 438.15 K of Fig. 1 are evaluated after correction with the asymmetry run. A typical linear curve is established and τ, evaluated. The same is done for the Al_2O_3 at 308.15 K. In order to calculate the heat capacity from Eq. (2), the amplitudes of the heat-flow rate $A_\Phi(\nu)$, for each harmonic frequency $\nu \times \omega$, and the corresponding sample-temperature amplitudes, $A_{T_s}(\nu)$, are deconvoluted using the Fourier transform to obtain the five harmonics of the complex sawtooth with approximately the same amplitudes given in Eq. (6). These were then inserted into Eq. (2). The ninth harmonic was not originally included in the analysis and has a somewhat smaller amplitude, but is still large enough to give useful data. The time constant τ and the τ-corrected heat capacity, C_p(c), were obtained according to Eq. (7). After correction, the heat capacity reaches a value with deviation of 0.1% from the literature and the ratio of both, 0.975, was used as the calibration constant for the PE fiber data. For the sapphire at 308.15 K, a τ was estimated to be 6.49 s rad^{-1} and the calibration constant as 0.92. The same procedure is repeated in Fig. 7 for the sample at 308.15 K, followed by the final step in the analysis, the correction with the factor with the sapphire experiment. The value of τ is 12.9 s rad^{-1} from the slope of only two points is indicated Fig. 7. The deviation of C_p(uc) is most likely due to the increased thermal resistance between the thin fibers among themselves and the pan, when compared to the Al_2O_3.

Fig. 8 illustrates the final data treatment for the PE fiber for 438.15 K using the results of Figs. 4 and 6. While Figs. 6 and 7 show the typical increasing of uncorrected heat capacity C_p(uc) with an increasing period, of the harmonics, Fig. 8 shows the opposite trend. Above the melting temperature, the value of τ^2 becomes negative, and a corrected heat capacity cannot be evaluated.

Fig. 9 displays the results from quasi-isothermally TMDSC with a single-frequency, sinusoidal modulation. The uncorrected data are too low when compared to the Data Bank values. Correction by internal calibration by shifting to agreement with the Data Bank in the liquid region yields too high a heat capacity below the melting temperature. The cooling and second heating runs, in contrast, give reasonable results. These data duplicate earlier measurements with a 2920® DSC [11]. The earlier measurements also could only be reconciled with the Data Bank over the whole temperature region by making two internal calibrations, one at low temperature, before deformation of the pan at 413.4 K, and one at high temperature, to correct for the

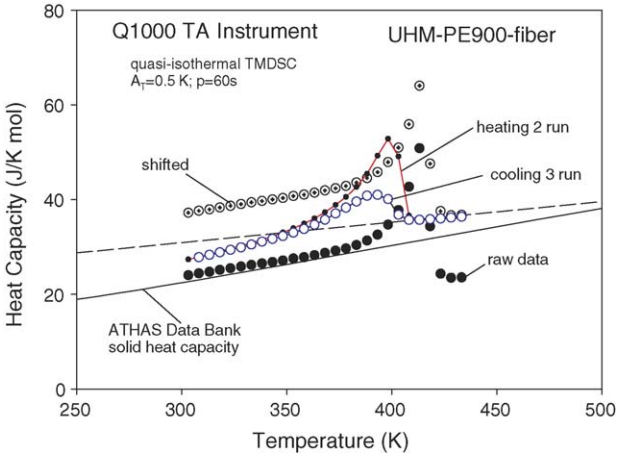

Fig. 9. Comparison of the results of quasi-isothermal TMDSC for the PE fibers. The data already displayed in Figs. 7 and 8 are labeled raw data. After correction at a single point in the melt these data are replotted as shifted. On subsequent cooling after the first heating and on a renewed, second heating and third cooling by continued measurement without change in the sample and without further correction no new shift is necessary.

deformation. This deformation could, in addition, be pinpointed at the melting peak [15]. The initial, smaller calibration error arises to the increased thermal resistance of the fibers. In the liquid state, the calibration error was due to the shrinkage of the fibers which deformed the pan in the melting process. The effect on τ^2 shown in Figs. 7 and 8, respectively, are a sensitive indication of these difficulties.

5. Conclusions

Four interesting points could be illustrated in the present paper. First, the results in Figs. 1, 2, 5, and 6 document that the simplified sawtooth can be used for high-precision measurements of the heat capacity of polymeric materials using the standard DSC mode. The newer Q1000® DSC offers a special advantage in not needing an asymmetry correction, which can, however, only be made use of if the corrected data can be exported or analyzed with the commercial software. The advantage of this procedure is to have identical experimental conditions and thermal history for all frequencies, a condition which cannot be attained with separate experiments at the different frequencies.

Second, the results for Fig. 8 in the liquid state, inadvertently measured with a strongly deformed pan, demonstrate that the complex sawtooth approaches a negative value of τ^2 and can be a sensitive probe to detect such experimental difficulties. The lowering of the uncorrected heat capacities with higher periods is related to the spikes in the heat-flow rates of PE fiber in the liquid state due to the deformation of the pan seen in Fig. 4. The sensitivity of the high-frequency analysis can be judged from Fig. 3, which shows negligible spikes in the heat-flow rate, but the analysis in Fig. 7 reveals already major deviations in the τ^2-plot at higher frequency.

Third, Fig. 2 illustrates the Tzero® calibration and the results suggests that a separate asymmetry correction can be avoided. Such correction is necessary with all other heat-flux and power-compensation DSCs.

Fourth, Fig. 9, proves that even with difficulties arising from the higher thermal resistance of deformed pans and small fibers (and powders and other high thermal-resistance samples), quantitative single-run TMDSC is possible when using an appropriately low frequency and an internal calibration. This also emphasizes the importance of the upkeep and expansion of appropriate data banks. Without a proper internal calibration, the measurement of Fig. 9 cannot yield useful data over the complete temperature range.

Acknowledgments

This work was financially supported by the Division of Materials Research, NSF, Polymers Program, Grant #DMR-0312233 and the Division of Materials Science, Office of Basic Energy Sciences, DOE at Oak Ridge National Laboratory, managed by Lockheed Martin Energy Research Corp. for DOE, under contract number DE-AC05-00OR22725.

References

[1] G.W.H. Hoehne, L. Kurelec, Thermochim. Acta 377 (2001) 141.
[2] G.W.H. Hoehne, L. Kurelec, S. Rastogi, P.J. Lemstra, Thermochim. Acta 396 (2003) 97.
[3] M. Pyda (Ed.), ATHAS Data Bank, http://web.utk.edu/~athas/databank.
[4] B. Wunderlich, Y. Jin, A. Boller, Thermochim. Acta 238 (1994) 277.
[5] A. Boller, Y. Jin, B. Wunderlich, J. Therm. Anal. 42 (1994) 307.
[6] R. Androsch, B. Wunderlich, Thermochim. Acta 333 (1999) 27.
[7] B. Wunderlich, R. Androsch, M. Pyda, Y.K. Kwon, Thermochim. Acta 348 (2000) 181.
[8] M. Pyda, Y.K. Kwon, B. Wunderlich, Thermochim. Acta 367–368 (2001) 217.
[9] Y.K. Kwon, R. Androsch, M. Pyda, B. Wunderlich, Thermochim. Acta 367–368 (2001) 203.
[10] Y.K. Kwon, A. Boller, M. Pyda, B. Wunderlich, Polymer 41 (2000) 6237.
[11] J. Pak, B. Wunderlich, Thermochim. Acta 421 (2004) 203.
[12] R.L. Danley, Thermochim. Acta 395 (2003) 201.
[13] K. Ishikiriyama, B. Wunderlich, J. Therm. Anal. 50 (1997) 337.
[14] A. Boller, I. Okazaki, K. Ishikiriyama, G. Zhang, B. Wunderlich, J. Therm. Anal. 49 (1997) 1081.
[15] J. Pak, W. Qiu, M. Pyda, E. Nowak-Pyda, B. Wunderlich, J. Thermal Anal., in press.